Sequential deposition method fabricating carbon-based fully-inorganic perovskite solar cells

Xihong Ding[1], Yingke Ren[1], Yahan Wu[1], Yafeng Xu[2], Jun Zhu[2,3*], Tasawar Hayat[4,5], Ahmed Alsaedi[4], Zhaoqian Li[2], Yang Huang[2] and Songyuan Dai[1,2*]

ABSTRACT   Hybrid organic-inorganic halide perovskite material has been considered as a potential candidate for various optoelectronic applications. However, their high sensitivity to the environment hampers the actual application. Hence the technology replacing the organic part of the hybrid solar cells needs to be developed. Herein, we fabricated fully-inorganic carbon-based perovskite $CsPbBr_3$ solar cells *via* a sequential deposition method with a power conversion efficiency of 2.53% and long-time stability over 20 d under ambient air conditions without any encapsulation. An evolution process from tetragonal $CsPb_2Br_5$ to $CsPb_2Br_5$-$CsPbBr_3$ composites to quasi-cubic $CsPbBr_3$ was found, which was investigated by scanning electron microscopy, X-ray diffraction spectra, UV-vis absorption spectra and Fourier transform infrared spectroscopy. Detailed evolution process was studied to learn more information about the formation process before 10 min. Our results are helpful to the development of inorganic perovskite solar cells and the $CsPb_2Br_5$ based optoelectronic devices.

Keywords: perovskite solar cell, phase transition, carbon cathode

INTRODUCTION

In the past several years, hybrid organic-inorganic halide perovskites with the common formulation ABX_3 (where A is an organic cation, B is commonly Pb^{2+} and X is a halide) have undergone breathtaking progress in power conversion efficiency (PCE) from nascent 3.8% [1] to a striking record of 22.1% [2]. Hybrid organic-inorganic halide perovskites have been verified to be in possession of many excellent properties, such as long electron/hole diffusion length [3], remarkable sunlight absorption [4], easy and low-cost fabrication process [5], etc., which make them an ideal candidate for lots of applications in photodetectors [6], light-emitting devices [7], semiconductor lasers [8], and solar cells [9–11].

However, the actual application of hybrid perovskites is hindered because of their strong sensitivity to ultraviolet (UV) light [12], heat [13], and moisture [14,15]. Fortunately, inorganic cesium lead halides, $CsPbX_3$ (X=Cl, Br, I) show prominent compositional stability under thermal stress and remarkable photoelectric features with high electron mobility up to ~1000 cm^2 V^{-1} s^{-1} [16]. In 2015, the first inorganic $CsPbBr_3$ perovskite solar cells (PSCs) were reported by Kulbak *et al.* [17], acquiring a PCE of about 5%. More recently, Liao *et al.* [18] reported $CsPbX_3$ nanowires stable solar cells with PCE of 1.21% and stability around 5500 h. Liang *et al.* [19] reported carbon-based $CsPbBr_3$ solar cells with a PCE of 6.7% and stability over three months in humid air (90%–95% relative humidity, 25°C). As for $CsPbI_3$, undesired orthorhombic phase was formed with a low PCE of 0.09% due to its poor phase stability to moisture [20]. $CsPb_2Br_5$ is another important material for optoelectronic applications. The advantages of $CsPb_2Br_5$ used in optoelectronic devices lie in the intrinsic sandwiched structure and physical properties from the structure. In the tetragonal $CsPb_2Br_5$ structure, one layer of Cs ions is sandwiched between two layers of Pb-Br coordination polyhedrons [21]. Now the applications of $CsPb_2Br_5$ include laser and

[1] Beijing Key Laboratory of Novel Thin-Film Solar Cells, North China Electric Power University, Beijing 102206, China
[2] Key Laboratory of Photovoltaic and Energy Conservation Materials, Hefei Institutes of Physical Science, Chinese Academy of Sciences, Hefei 230031, China
[3] Key Lab of Special Display Technology, Ministry of Education, National Engineering Lab of Special Display Technology, State Key Lab of Advanced Display Technology, Academy of Opto-Electronic Technology, Hefei University of Technology, Hefei 230009, China
[4] NAAM Research Group, Department of Mathematics, Faculty of Science, King Abdulaziz University, Jeddah 21589, Saudi Arabia
[5] Department of Mathematics, Quaid-I-Azam University, Islamabad 44000, Pakistan
* Corresponding authors (emails: zhujzhu@gmail.com (Zhu J); sydai@ipp.ac.cn (Dai S))
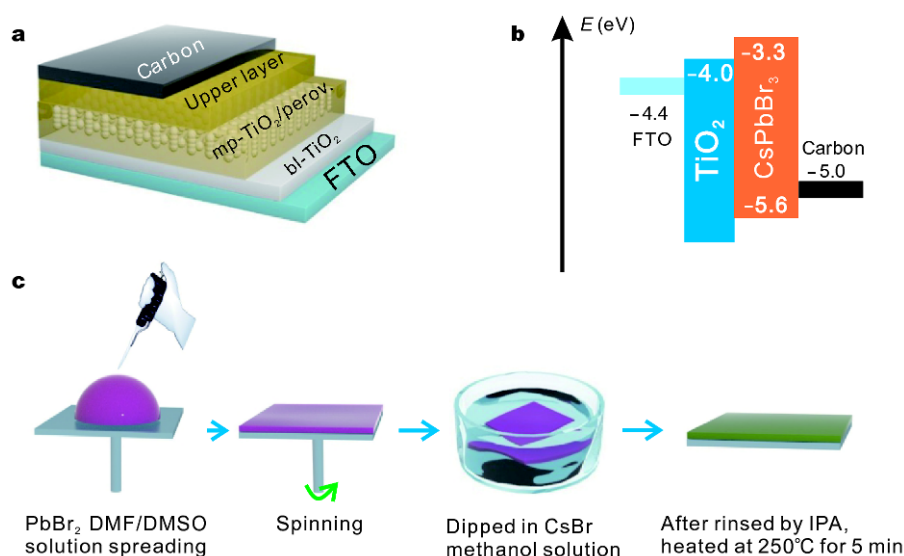
Figure 1 (a) Device architecture of CsPbBr$_3$/carbon based all-inorganic PSCs (glass/FTO/bl-TiO$_2$/ms-TiO$_2$-perovskite nanocomposite layer/perovskite upper layer/carbon); (b) energy level diagram of CsPbBr$_3$/carbon based all-inorganic PSCs; (c) scheme view of fabrication process of the perovskite film using sequential deposition method.

light-emitting devices [22–24]. Compared with the perovskite CsPbBr$_3$, the available research on the structure and physical properties of the tetragonal CsPb$_2$Br$_5$ is not very sufficient and many great blanks need to be filled [21]. Our results offer a facile way to synthesize CsPb$_2$Br$_5$, which could enlighten other researchers to develop and design more applications of CsPb$_2$Br$_5$. At the same time, we use sequential deposition method obtaining CsPbBr$_3$ films using carbon as hole-transporting material and photocathode, achieving a PCE of 2.53% with long-term stability. Scanning electron microscopy (SEM), X-ray diffraction spectra (XRD), Fourier transform infrared spectroscopy (FT-IR) and UV-vis absorption spectra were used to investigate CsPb$_2$Br$_5$, CsPbBr$_3$ and the transition from CsPb$_2$Br$_5$ to CsPbBr$_3$. Our results are helpful to the development of fully-inorganic CsPbBr$_3$ solar cells and CsPb$_2$Br$_5$ based optoelectronic device.

EXPERIMENTAL SECTION

Materials
F-doped SnO$_2$ glass (FTO, 15 Ω/square) was purchased from Pilkington TEC. Lead bromide (PbBr$_2$, ≥98%), N,N-dimethylformamide (DMF) and dimethyl sulphoxide (DMSO) were obtained from Aldrich. Cesium bromide (CsBr, >99%) was purchased from TCI. TiO$_2$ (particle size: about 30 nm, crystalline phase: anatase) was purchased from Dyesol. Methanol (AR) and isopropanol (IPA, 99.7%) were obtained from Sinopharm Chemical

Reagent Co., Ltd. All chemicals were straightly used without further purification.

Device fabrication
Etched FTO-coated glass substrates were cleaned by ultrasonication in deionized water followed by washed with acetone and ethanol. These substrates were exposed to UV-ozone for 15 min. A ~60 nm-thick TiO$_2$ blocking layer was deposited on the cleaned FTO by spray pyrolysis, using N$_2$ as carrier gas, at 430°C from a precursor solution of 0.6 mL of titanium diisopropoxide and 0.4 mL of bis(acetylacetonate) in 7 mL of anhydrous isopropanol. A mesoporous TiO$_2$ layer (particle size: about 30 nm, crystalline phase: anatase, diluted to w/w=1/5.5 in ethanol) about 100–150 nm thickness film was deposited by spin coating at 5000 rpm for 30 s onto the blocking layer (bl)-TiO$_2$/FTO substrates. After spin coating, the substrate was immediately dried on a hotplate at 105°C, and the substrates were then heated at 500°C to remove organic components followed by baking for 2 h. Then, as illustrated in Fig. 1c, firstly, 1.4 mol L^{-1} PbBr$_2$ DMF/DMSO solution (DMF/DMSO v/v=9/1) was spread over the entire surface of the substrate. Secondly, the spin-coater was accelerated to the desired rotational speed at 2000 rpm for 30 s. Thirdly, the as-prepared PbBr$_2$ films were dipped into 15 mg mL^{-1} CsBr methanol solution for various time. Finally, the perovskite films were rinsed by IPA and heated at 250°C for 5 min. Then, the carbon paste was deposited on the perovskite films by screen
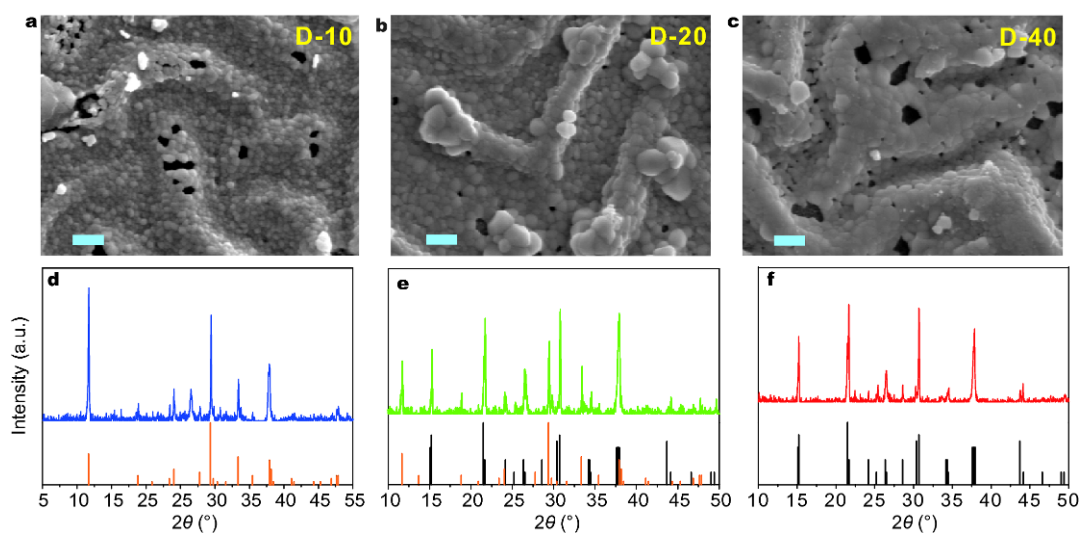
Figure 2 SEM Images of inorganic active layer: (a) D-10; (b) D-20; (c) D-40; the scale bar is 1 μm and XRD patterns of D-10 (d), D-20 (e), D-40 (f) with standard XRD patterns, orange line: tetragonal $CsPb_2Br_5$, JCPDS No. 00-025-0211; black line: monoclinic $CsPbBr_3$, JCPDS No. 00-018-0364.

printing followed by heating at 70°C for 1 h.

Characterization

Film morphology was investigated by using a high-resolution scanning electron microscope (S4800, Hitachi) equipped with a Schottky Field Emission gun. The X-ray diffraction spectra were recorded on an X'pert PRO X-ray diffractometer. The data were gathered at room temperature in the 2θ range 5°–50°. The *J-V* curves were measured using a solar simulator (Newport, Oriel Class A, 91195A) with a source meter (Keithley 2420) at 100 mA cm^{-2} illumination AM 1.5 G and a calibrated Si-reference cell. The *J-V* curves for all devices were measured by masking the active area with a black mask 0.09 cm^2. The applied bias voltage was from 1.2 to –0.1 V and the scan rate was 50 mV s^{-1}. UV-vis absorption spectra were recorded on a UV-vis spectrometer (Hitachi U-3300). Fourier transform infrared spectroscopy (FT-IR, ThermoFisher IS50R, USA) was used to collect the spectral data for various solution in the range of 4000–500 cm^{-1}.

RESULTS AND DISCUSSION

Structure and morphology characterization

Fig. 1 presents the device architecture, energy level diagram as well as scheme of films fabrication process. The cell structure (Fig. 1a) exhibits a bilayer structure making up of mesoporous and planar structures, which is effective for adequately absorbing light and gathering charges.

Atop the mesoporous (mp)-TiO_2 layer lies a uniform perovskite active layer. Upward the perovskite active layer lies a layer of carbon working as bi-functional films for both electron blocking and hole collecting for the reason of its fit work function (–5.0 eV) close to that of gold (–5.1 eV). Fig. 1b exhibits the energy band diagram of FTO, TiO_2, $CsPbBr_3$ and carbon layers, uncovering the smooth electron injection from $CsPbBr_3$ conduction band to TiO_2 conduction band and hole extraction from $CsPbBr_3$ valence band to carbon photocathode. Fig. 1c shows the perovskite films fabrication process, in which the as-prepared $PbBr_2$ films was dipped in 15 mg mL^{-1} CsBr methanol solution for 10 (D-10), 20 (D-20) and 40 min (D-40).

The surface morphology evolution of the inorganic active layer based on different dipping time was investigated by SEM (Fig. 2a–c). The films dipped in CsBr methanol solution for 10 min (D-10) exhibit relatively low surface coverage and small grain size (the average grain size is 216 nm calculated by software Nanomeasurer with 30 sample points.) The D-20 film is relatively more uniform with average grain size of 275 nm. For the D-40 film, the average grain size becomes larger up to 391 nm. Our results show that longer dipping time is beneficial for better performance of the $CsPbBr_3$ PSCs. It is worthy to note that all the three kinds of films have lots of fluctuation, which is detrimental to electron and hole transfer. The cause of the fluctuation is unclear and need to be further studied. Fig. S1 (Supplementary information) illustrates the carbon photocathode, which shows it com-

prised carbon nanoparticles with average diameter of ~100 nm.

The XRD measurement was conducted to investigate the crystal phase evolution of these samples. As depicted in Fig. 2d, the XRD pattern of D-10 films could match well with standard patterns of tetragonal phase $CsPb_2Br_5$ (JCPDS No. 00-025-0211), whose lattice parameters are $a=b=8.483$ Å, $c=15.250$ Å, $\alpha=\beta=\gamma=90.000°$. Along with the prolonging of dipping time, as shown in Fig. 2e, a different material and phase emerged in the D-20 films, which is ascribed to monoclinic phase $CsPbBr_3$ (JCPDS No. 00-018-0364), with lattice parameters $a=b=5.827$ Å, $c=5.891$ Å, $\alpha=\beta=90.000°$, $\gamma=89.650°$. It is quite similar as cubic phase with slight difference of c and γ, so we call this structure as quasi-cubic phase $CsPbBr_3$. In the D-20 films, the XRD peaks belong to two kinds of materials (tetragonal $CsPb_2Br_5$ and quasi-cubic $CsPbBr_3$), indicating the material and phase evolution is in progress and the $CsPb_2Br_5$ has not completely evolved to $CsPbBr_3$. However, when we turn to the D-40 films, as illustrated in Fig. 2f, all the $CsPb_2Br_5$ converts to $CsPbBr_3$. It is worthy to note that no peak of $PbBr_2$ could be found, indicating the sufficient reaction of $PbBr_2$ and CsBr with no $PbBr_2$ residual remained in all the three kinds of films. Fig. S2 shows absorbance of the D-10, D-20 and D-40 films. The light absorption peaks of D-20 and D-40 films are shorter than ~540 nm and the absorption peak of D-10 films is shorter than ~375 nm, which suggests tetragonal $CsPb_2Br_5$ was not suitable for photovoltaic applications.

To learn more information about the formation process at the interface of $PbBr_2$ films and the CsBr methanol solution before 10 min, we investigated the as-prepared $PbBr_2$ films dipped in the 15 mg mL^{-1} CsBr methanol solution for 1 (D-1), 2 (D-2) and 5 min (D-5). XRD measurement and UV-vis spectra were used to further investigate $CsPb_2Br_5$. As depicted in Fig. 3a, the XRD patterns of D-1, D-2 and D-5 have slight difference in the intensity, while all matching well with the standard XRD pattern ($CsPb_2Br_5$ JCPDS No. 00-025-0211), indicating that even early at 1 min, the tetragonal $CsPb_2Br_5$ was formed at the interface. It is worthy to note that the full width at half maxima (FWHM) of XRD patterns of D-1, D-2 and D-5 films are wider than that of D-10, showing smaller grainsize compared with the D-10 films according to Debye-Scherrer formula. As presented in Fig. S3, the light absorption peaks of these films are shorter than ~375 nm.

Combining the previous reports [21,22,25] and the fact that no $PbBr_2$ residual could be found in D-10 films, we hypothesize the reaction route according to the equation:

$CsBr+2PbBr_2 \rightarrow CsPb_2Br_5$. Then, $CsPb_2Br_5$ continues to react with CsBr in methonal according to the equation: $CsPb_2Br_5+CsBr \rightarrow 2CsPbBr_3$. In the first step, the effect of the $PbBr_2 \cdot DMF$ adduct is considered to be important for the formation of $CsPb_2Br_5$. Without the existence of the adduct, the reaction process should be different [19,26]. FT-IR was conducted to confirm the existence of the adduct. As depicted in Fig. 3b, the stretching vibrations of C=O in DMF and DMSO (v/v=9:1) mixed solution (T-1 solution) were located at 1670 cm^{-1}. When 513.8 mg $PbBr_2$ was added to 1 mL T-1 solution (T-2 solution), some of the vibrations of C=O shifted to 1638 from 1670 cm^{-1}, which could prove the existence of $PbBr_2 \cdot DMF$ adduct.

Photovoltaic performance

The photovoltaic application of perovskite has recently become a hotspot. In consideration of this, we fabricated the PSCs based on D-10, D-20, D-40 films. Table 1 summarizes the typical photovoltaic properties of the three kinds of solar cells. Unfortunately, the device based on D-10 films did not perform photovoltaic properties because of its broad band gap. However, we propose a new strategy to synthesis $CsPb_2Br_5$ here, which will help other researchers to expand its application in other fields. The devices based on D-20 films show a relatively low open circuit voltage (V_{oc}), short current density (J_{sc}), PCE, and fill factor (FF) comparing with the devices based on D-40 films because of the existence of $CsPb_2Br_5$. The best cell based on D-40 films, as depicted in Fig. 3c, yielded a J_{sc} of 3.52 mA cm^{-2}, a V_{oc} of 1.15 V, an FF of 0.624 and a PCE of 2.53%. Fig. 3d presents the cross-sectional SEM image of the device based on D-40 films, signifying a structure making up of FTO, 60 nm-thick bl-TiO_2, 200 nm-thick meso-TiO_2/perov., 650 nm-thick upper layer and carbon photocathode.

Stability of devices

The stability of solar cells is of fundamental importance to the commercialization process. Stability is still a challenge for the hybrid PSCs [27]. Herein the stability test of the devices based on D-40 films were conducted under ambient air without any encapsulation. Fig. 3e illustrates normalized stability curves of the device based on D-40 films, which shows that the PSCs were stable after 20 d. Prominent stability will be beneficial to the commercial application process.

CONCLUSION

In summary, we proposed a simple sequential deposition
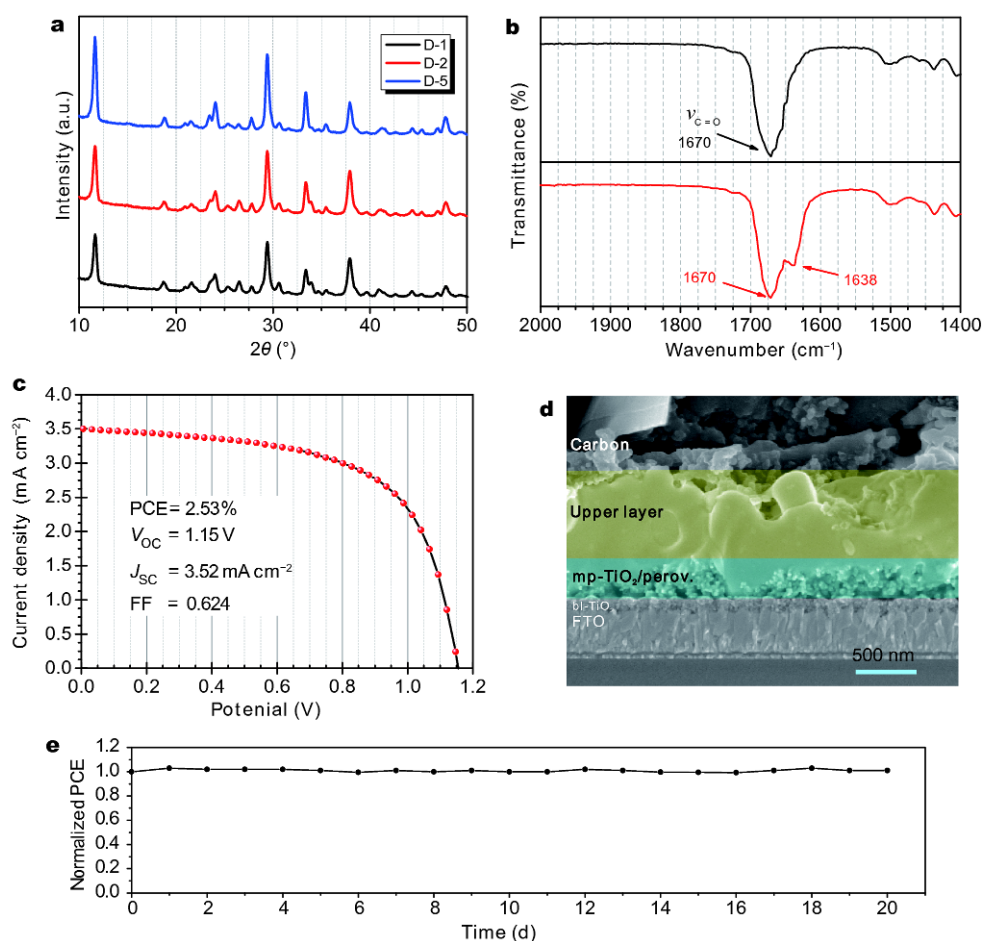
Figure 3 (a) XRD patterns of D-1, D-2, D-5 films; (b) FT-IR of T-1 solution (black line) and T-2 solution (red line); (c) champion cell's *J-V* characteristics of the PSC devices based on D-40 films; (d) cross-sectional SEM image of a full cell based on D-40 films, the scale bar is 500 nm; (e) normalized PCE of the device based on D-40 films.

Table 1 Typical device performance of PSCs

	J_{sc} (mA cm^{-2})	V_{oc} (V)	PCE (%)	FF
D-10	–	–	–	–
D-20	1.89	0.83	0.82	0.52
D-40	3.25	1.10	2.18	0.61

method to fabricate fully-inorganic PSCs using carbon as hole-transporting material and photocathode. A material and phase evolution process from tetragonal $CsPb_2Br_5$ to quasi-cubic $CsPbBr_3$ was found and characterized. SEM, XRD patterns, UV-vis spectra and FT-IR spectra were used to investigate the evolution process. We proposed a hypothesis to explain the evolution process. The best cell based on quasi-cubic $CsPbBr_3$ films presented a PCE of 2.53% with long stability over 20 d under ambient air conditions without any encapsulation. Our results are helpful to the development of $CsPbBr_3$ based PSCs. In

addition, the facile way to synthesize $CsPb_2Br_5$ could enlighten other researchers to develop and design more applications of it.

1 Kojima A, Teshima K, Shirai Y, *et al*. Organometal halide perovskites as visible-light sensitizers for photovoltaic cells. J Am Chem Soc, 2009, 131: 6050–6051

2 http://www.nrel.gov/ncpv/images/efficiency_chart.pn. 2017.7.5

3 Dong Q, Fang Y, Shao Y, *et al*. Electron-hole diffusion lengths>175 μm in solution-grown CH₃NH₃PbI₃ single crystals. Science, 2015, 347: 967–970

4 Ren Y, Duan B, Xu Y, *et al*. New insight into solvent engineering technology from evolution of intermediates *via* one-step spin-coating approach. Sci China Mater, 2017, 60: 392–398

5 Lee JW, Kim HS, Park NG. Lewis acid-base adduct approach for high efficiency perovskite solar cells. Acc Chem Res, 2016, 49: 311–319

6   Tan ZK, Moghaddam RS, Lai ML, *et al.* Bright light-emitting diodes based on organometal halide perovskite. Nat Nanotech, 2014, 9: 687–692

7   Wang Z, Cheng T, Wang F, *et al.* Morphology engineering for high-performance and multicolored perovskite light-emitting diodes with simple device structures. Small, 2016, 12: 4412–4420

8   Xing G, Mathews N, Lim SS, *et al.* Low-temperature solution-processed wavelength-tunable perovskites for lasing. Nat Mater, 2014, 13: 476–480

9   Seo J, Noh JH, Seok SI. Rational strategies for efficient perovskite solar cells. Acc Chem Res, 2016, 49: 562–572

10 Li ZQ, Que YP, Mo LE, *et al.* One-pot synthesis of mesoporous TiO_2 microspheres and its application for high-efficiency dye-sensitized solar cells. ACS Appl Mater Interfaces, 2015, 7: 10928–10934

11 Li ZQ, Chen WC, Guo FL, *et al.* Mesoporous TiO_2 yolk-shell microspheres for dye-sensitized solar cells with a high efficiency exceeding 11%. Sci Rep, 2015, 5: 14178

12 Leijtens T, Eperon GE, Pathak S, *et al.* Overcoming ultraviolet light instability of sensitized TiO_2 with meso-superstructured organometal tri-halide perovskite solar cells. Nat Commun, 2013, 4: 2885

13 Conings B, Drijkoningen J, Gauquelin N, *et al.* Intrinsic thermal instability of methylammonium lead trihalide perovskite. Adv Energ Mater, 2015, 5: 1500477

14 Manser JS, Saidaminov MI, Christians JA, *et al.* Making and breaking of lead halide perovskites. Acc Chem Res, 2016, 49: 330–338

15 Liu X, Kong F, Cheng T, *et al.* Tetraphenylmethane-arylamine hole-transporting materials for perovskite solar cells. ChemSusChem, 2017, 10: 968–975

16 Stoumpos CC, Malliakas CD, Peters JA, *et al.* Crystal growth of the perovskite semiconductor $CsPbBr_3$: a new material for high-energy radiation detection. Cryst Growth Des, 2013, 13: 2722–2727

17 Kulbak M, Cahen D, Hodes G. How important is the organic part of lead halide perovskite photovoltaic cells? Efficient $CsPbBr_3$ cells. J Phys Chem Lett, 2015, 6: 2452–2456

18 Liao JF, Li WG, Rao HS, *et al.* Inorganic cesium lead halide $CsPbX_3$ nanowires for long-term stable solar cells. Sci China Mater, 2017, 60: 285–294

19 Liang J, Wang C, Wang Y, *et al.* All-inorganic perovskite solar cells. J Am Chem Soc, 2016, 138: 15829–15832

20 Ripolles TS, Nishinaka K, Ogomi Y, *et al.* Efficiency enhancement by changing perovskite crystal phase and adding a charge extraction interlayer in organic amine free-perovskite solar cells based on cesium. Sol Energ Mater Sol Cells, 2016, 144: 532–536

21 Li G, Wang H, Zhu Z, *et al.* Shape and phase evolution from $CsPbBr_3$ perovskite nanocubes to tetragonal $CsPb_2Br_5$ nanosheets with an indirect bandgap. Chem Commun, 2016, 52: 11296–11299

22 Tang X, Hu Z, Yuan W, *et al.* Perovskite $CsPb_2Br_5$ microplate laser with enhanced stability and tunable properties. Adv Opt Mater, 2017, 5: 1600788

23 Wang KH, Wu L, Li L, *et al.* Large-scale synthesis of highly luminescent perovskite-related $CsPb_2Br_5$ nanoplatelets and their fast anion exchange. Angew Chem Int Ed, 2016, 55: 8328–8332

24 Zhang X, Xu B, Zhang J, *et al.* All-inorganic perovskite nanocrystals for high-efficiency light emitting diodes: dual-phase $CsPbBr_3$-$CsPb_2Br_5$ composites. Adv Funct Mater, 2016, 26: 4595–4600

25 Dastidar S, Egger DA, Tan LZ, *et al.* High chloride doping levels stabilize the perovskite phase of cesium lead iodide. Nano Lett, 2016, 16: 3563–3570

26 Hoffman JB, Schleper AL, Kamat PV. Transformation of sintered $CsPbBr_3$ nanocrystals to cubic $CsPbI_3$ and gradient $CsPbBr_xI_{3-x}$ through halide exchange. J Am Chem Soc, 2016, 138: 8603–8611

27 Chen H. Two-step sequential deposition of organometal halide perovskite for photovoltaic application. Adv Funct Mater, 2017, 27: 1605654

Author contributions   Ding X conducted the main experiments and wrote this manuscript. Zhu J directly guided this research including the designing, modifying and optimizing work related to this manuscript. Dai S supervised the projects and carefully reviewed and modified this manuscript. Ren Y, Wu Y, Xu Y, Tasawar H, Ahmed A, Li Z, Huang Y provided help in the fabrication of devices and methods of characterization. All authors contributed to the general discussion about this work.

Conflict of interest   The authors declare that they have no conflict of interest.

Supplementary information   Supporting data are available in the online version of the paper.

Xihong Ding gained his BSc degree from North China Electric Power University in 2015. He is now a PhD candidate of the North China Electric Power University under the supervision of Profs. Jun Zhu and Songyuan Dai. His research interests mainly focus on perovskite solar cells.
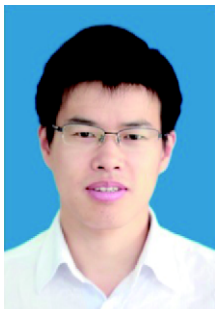
Jun Zhu received his PhD degree from University of Science and Technology of China in 2005. He joined Hefei Institutes of Physical Science, Chinese Academy of Sciences and was promoted to full professor in 2015. Now his research interests focus on the new generation solar cells, including quantum dot solar cells and perovskite solar cells.

Songyuan Dai is a professor and Dean of the School of Renewable Energy, North China Electric Power University. He obtained his BSc degree in physics from Anhui Normal University in 1987, and MSc and PhD degrees in plasma physics from the Institute of Plasma Physics, Chinese Academy of Sciences in 1991 and 2001. His research interests mainly focus on next-generation solar cells including dye-sensitized solar cells, quantum dot solar cells, perovskite solar cells, etc.

连续沉积法制备碳电极无机钙钛矿太阳电池

丁希宏[1]，任英科[1]，吴雅罕[1]，徐亚峰[2]，朱俊[2,3*]，Tasawar Hayat[4,5]，Ahmed Alsaedi[4]，李兆乾[2]，黄阳[2]，戴松元[1,2*]

摘要 有机无机杂化钙钛矿是一种有潜力的光伏材料. 然而，对于环境的高度敏感性限制了它的实际应用. 因此我们需要发展全无机钙钛矿材料. 本文通过连续沉积法制备了效率达到2.53%的碳电极$CsPbBr_3$太阳电池，并且它能够在无封装的情况下稳定20天. 在制备$CsPbBr_3$薄膜的过程中，我们首次发现从$CsPb_2Br_5$到$CsPb_2Br_5$-$CsPbBr_3$混合物到$CsPbBr_3$的转变. 该研究结果对于无机钙钛矿太阳电池的发展和$CsPb_2Br_5$基光电器件具有帮助作用.